

See discussions, stats, and author profiles for this publication at: <https://www.researchgate.net/publication/271599247>

Self-Assembly of Responsive Multilayered DNA Nanocages

ARTICLE *in* JOURNAL OF THE AMERICAN CHEMICAL SOCIETY · JANUARY 2015

Impact Factor: 12.11 · DOI: 10.1021/ja5101307 · Source: PubMed

CITATIONS

3

READS

80

6 AUTHORS, INCLUDING:



[Cheng Tian](#)

Purdue University

25 PUBLICATIONS 138 CITATIONS

[SEE PROFILE](#)



[Jinwen Yu](#)

Purdue University

6 PUBLICATIONS 110 CITATIONS

[SEE PROFILE](#)



[Wen Jiang](#)

Purdue University

95 PUBLICATIONS 3,947 CITATIONS

[SEE PROFILE](#)



[Chengde Mao](#)

Purdue University

136 PUBLICATIONS 6,335 CITATIONS

[SEE PROFILE](#)

Self-Assembly of Responsive Multilayered DNA Nanocages

Zhiyu Liu,[†] Cheng Tian,[†] Jinwen Yu,[†] Yulin Li,[†] Wen Jiang,[‡] and Chengde Mao^{*,†}

[†]Department of Chemistry and [‡]Markey Center for Structural Biology and Department of Biological Sciences, Purdue University, West Lafayette, Indiana 47907, United States

Supporting Information

ABSTRACT: Here we report the assembly of multilayered DNA nanocages. The layers can be separated in response to a chemical cue, ATP. This is an effort to increase the structural complexity of DNA nanocages. The structures have been characterized by native polyacrylamide gel electrophoresis, atomic force microscopy, and cryogenic electron microscopy. We envision that the layer-by-layer assembly strategy used in this study can be easily applied to other DNA nanocages to form Russian-doll-like semisolid structures, while the chemically activated layer separation makes a contribution to the development of “smart” DNA nanocages.

DNA has been exploited to construct various DNA nanostructures over the last three decades.^{1–3} Among them, DNA nanocages have attracted great interest and effort on account of their potential capability to serve as capsules for cargo delivery.^{4,5} Several self-assembly strategies for DNA nanocages have been developed, for instance, tile-based assembly⁶ and DNA origami.⁷ However, the complexity and functionalization of DNA nanocages remain to be improved before their applications can thrive. Inspired by multiwalled carbon nanotubes and the layer-by-layer assembly method, we report a stepwise strategy to fabricate “Russian doll”-like multilayered DNA tetrahedra, followed by ATP-activated layer separation.

We have assembled Russian-doll-like DNA nanocages in a layer-by-layer fashion from inside to outside (Figure 1). The structures are named according to the number of layers: single-layered tetrahedron (sTET), double-layered TET (dTET), and triple-layered TET (tTET). Each layer is a tetrahedral structure, named as TET¹, TET², and TET³ for the first, second, and third layers, respectively. Superscript numbers indicate the layer numbers from inside to outside, e.g. “1” indicates the innermost layer. The layers are similar in structure but different in size. The basic motifs used are three-point-star motifs (Y¹, Y², and Y³ for the first, second, and third layers, respectively). To accommodate the size difference of TETs in different layers, two spacer motifs (a double-crossover motif (DX²) for TET² and an elongated double-crossover motif (eDX³) for TET³) are used between the three-point-star motifs in the outside two layers. Each motif contains multiple DNA strands (Figure 1b), but some strands are related to each other by rotational symmetries (threefold rotational symmetry in the three-point-star motif and twofold rotational symmetry in the DX and eDX motifs); thus, those strands will have the same sequences.

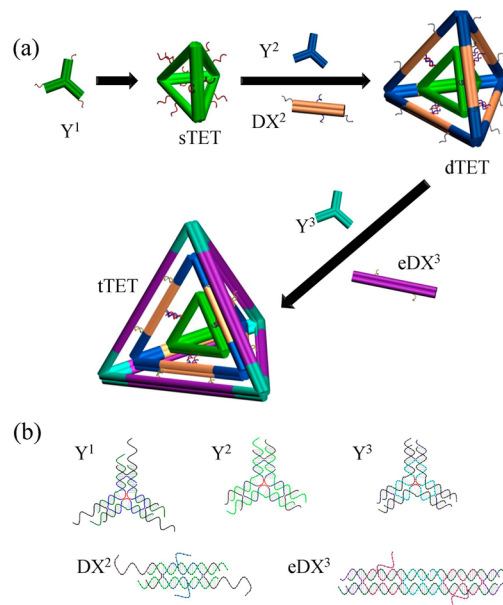


Figure 1. Layer-by-layer self-assembly of a multilayered DNA tetrahedron (TET). (a) The single-, double-, and triple-layered TETs are dubbed as sTET, dTET, and tTET, respectively. The building motifs are three-point-star (Y), double-crossover (DX), and elongated double-crossover (eDX) motifs. Superscript numbers indicate the layer numbers from inside to outside. For example, TET³ indicates the third (outermost)-layer TET, and Y³ indicates the three-point-star motif used for the assembly of TET³. Colored rods and thin lines represent DNA duplexes and single strands, respectively. (b) The detailed structures of the building motifs were drawn with Tiamat.⁸

There are duplex bridges between adjacent layers. Each TET layer has single-stranded tails. Between any two adjacent layers, the tails have complementary sequences and are carefully positioned in design so that the tails can hybridize with each other to connect the two layers.

The assembly needs multiple steps. First, individual DNA motifs and TET¹ are separately assembled by slowly cooling the corresponding DNA solutions from 95 to 4 °C over 16 h. Then the preassembled, individual DNA motifs are added to the solution of TET¹ and isothermally incubated at 37 °C to assemble the larger structures. Several isothermal incubation steps are involved, and only one type of individual motif is added during each step.

Received: October 1, 2014

Published: January 28, 2015

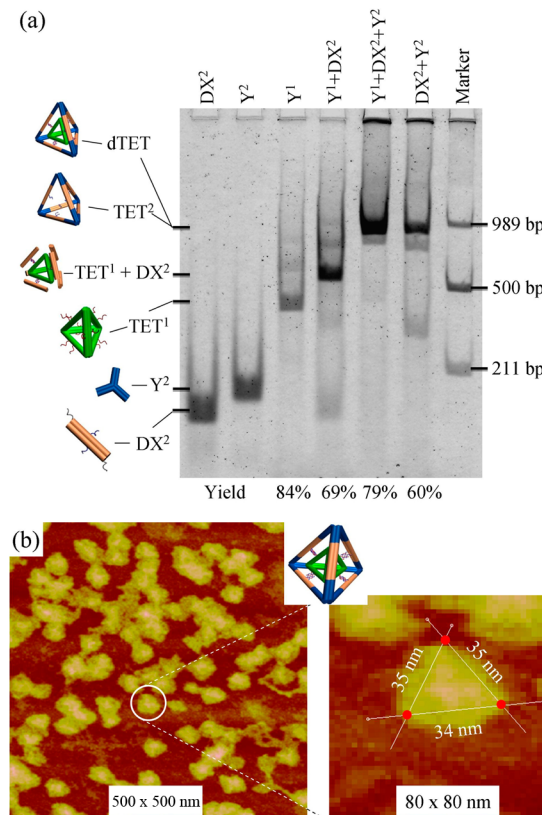


Figure 2. Characterization of the assembly of double-layered tetrahedron (dTET). (a) Native PAGE. The chemical composition of each sample is indicated above the gel image, and the chemical identity of each band is suggested beside the gel. The assembly yield of the target structure in each lane is indicated below the gel. (b) Atomic force microscopy: (left) typical AFM image; (right) close-up view of one particle with its three sides measured. It should be noted that AFM shows larger apparent lateral sizes at low-nanometer scale as a result of AFM tip convolution.

To test the strategy, we first assembled a double-layered TET (dTET), which was analyzed by native polyacrylamide gel electrophoresis (PAGE) (Figure 2a). The electrophoretic mobility of the products decreased as DX^2 motifs and Y^2 motifs were successively attached onto TET^1 , which matched well with the prediction based on the trend in increasing geometrical size and molecular weight. One interesting observation was that dTET traveled almost the same distance as TET^2 alone. Though these two DNA complexes had very different molecular weights, their overall sizes and exterior shapes were exactly the same. The assembly yield was quite high at each step. Single-layered TET^1 had the highest yield ($\sim 84\%$). When DX^2 motifs were mixed with TET^1 , the association was not complete. Interestingly, upon further addition of Y^2 motif to form the full double-layered tetrahedron, the assembly yield was quite high ($\sim 79\%$). It should be noted that each DX^2 motif was designed to have two tails that could anchor on the strut of TET^1 . In the absence of Y^2 motifs, there were no connections among DX^2 motifs. The interaction between each DX^2 motif and TET^1 was not strong enough to hold DX^2 on TET^1 . Thus, the TET^1 - DX^2 complex was a pretty floppy structure and not very stable. On the other hand, the assembly yield of single-layered TET^2 ($Y^2 + DX^2$) was also not very high ($\sim 60\%$). To some extent, the inside TET^1 acted as a structural scaffold for the outside TET^2 .

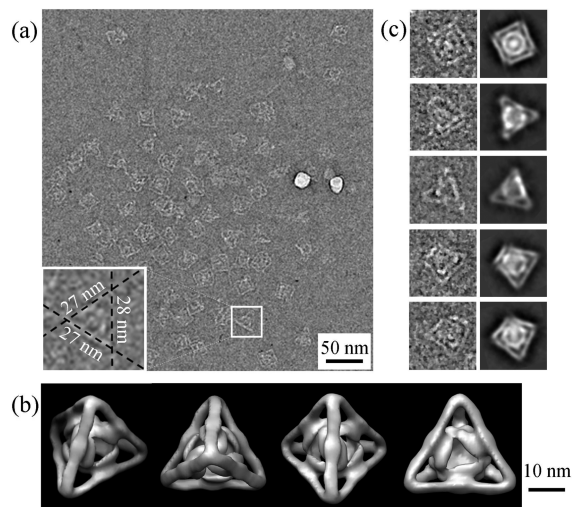


Figure 3. CryoEM study of dTET. (a) Typical CryoEM image displaying the expected double-layer feature. The inset shows the dimensions of one typical particle. For a clearer view, an enlarged version of the raw cryoEM image is included as Figure S1 in the Supporting Information. (b) Reconstructed 3D density map viewed from four different orientations. (c) Pairwise comparison between individual raw particle images and 2D projections back-calculated from the reconstructed 3D density map.

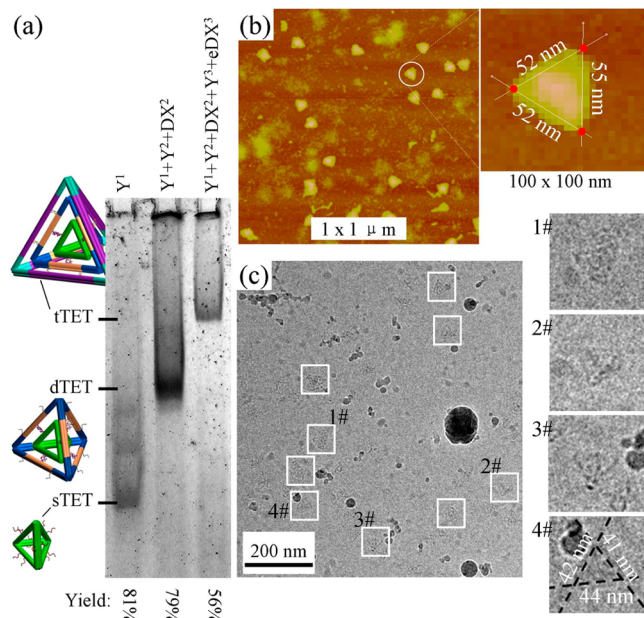


Figure 4. Characterization of the assembly of triple-layered tetrahedron (tTET). (a) Native PAGE. The chemical composition of each sample is indicated above the gel image, and the chemical identity of each band is suggested beside the gel. (b) AFM images. The dimensions of one typical particle are shown in the right image. (c) CryoEM image and close-up views of four individual particles. An enlarged version is included as Figure S3 in the Supporting Information for a clearer view. The dimensions of one typical particle (#4) are also shown.

Therefore, the lack of assistance from TET^1 explained the inefficient assembly of TET^2 . Only when all of the pieces (TET^1 , DX^2 , and Y^2) were fit into the right places in the puzzle could the connections within the second layer as well as the ones between the layers be fully established, ensuring the

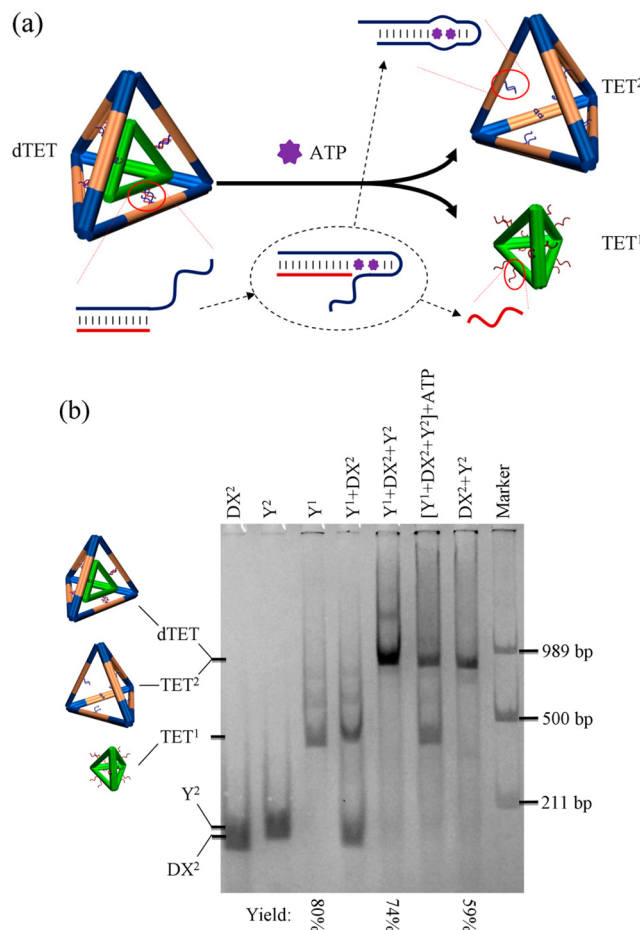


Figure 5. ATP-activated layer separation. (a) Separation mechanism. An ATP aptamer is embedded into the linkages between two TET layers. In the absence of ATP, the aptamer sequence (blue strand) on TET² hybridizes with the single strand tail (red strand) on TET¹ to provide the linkage between the two layers. In the presence of ATP, the aptamer binds to ATP and dissociates from the tail on TET¹, leading to separation of the two TET layers. (b) Experimental validation of the layer separation by native PAGE.

assembly of a structurally well-defined double-layered DNA nanocage.

To reveal the structure of the assembled dTET, we applied both atomic force microscopy (AFM) and cryogenic electron microscopy (CryoEM) to image the DNA complex. For AFM imaging, we used tapping mode in air to ensure that the DNA nanocages were firmly attached onto the substrate surface, which minimized the influence of the AFM probe. In the raw AFM images, uniformly sized individual DNA particles were randomly distributed (Figure 2b). In zoomed-in images, the semisolid DNA particles resembled the expected tetrahedral shape, and the center part was significantly higher than the peripheral region, consistent with the situation that a dTET collapsed on the mica surface (as a result of dehydration and strong DNA–mica interactions). We further applied CryoEM to image the dTET (Figure 3). CryoEM was an excellent tool to study such soft biomacromolecular complexes. In the raw images, distinct particles with the expected size were randomly distributed. The two signature traits of the target structure, the double-layered structure and tetrahedral appearance, could be identified even from the raw particles by the naked eye. Using single-particle three-dimensional (3D) reconstruction,^{9,10} we

were able to reveal the native 3D structure of the DNA complex as a double-layered tetrahedral object at 3.8 nm resolution (Figure 3b). One important feature displayed by the reconstructed structure was the linkages between the first and second layers. Consistent with the design, the struts of both layers were mutually connected at the middle part in a semiparallel manner. Furthermore, pairwise comparisons were conducted on the 2D projections generated from the reconstructed model with (i) raw images of individual particles (Figure 3c) and (ii) the class averages of raw particle images with the same orientation (Figure S2 in the Supporting Information). The clear similarity verified the reconstructed structural model. We noticed that the struts of the inside TET (TET¹) in the reconstructed model seemed to be much wider than expected. This indicated that the linkages between the two layers were not completely fixed. Relative to the outer TET², the inner TET¹ had certain degrees of freedom that led to the broadening of the struts of TET¹.

Inspired by the successful assembly of dTET, we went further to assemble a triple-layered tetrahedron (tTET). The linkages between the second and third layers were placed at the 1/4 and 3/4 points of each strut on the second layer and the 1/3 and 2/3 points of each strut on the third layer. The PAGE analysis included the DNA complexes corresponding to sTET, dTET, and tTET (Figure 4a). Each sample showed one major band corresponding to the DNA complexes. The electrophoretic mobility monotonically decreased as the molecular weight of the DNA complex increased. However, the assembly yield of tTET was significantly lower than those of sTET and dTET, and some quite large aggregates formed, which could not penetrate into the PAGE gel matrix. This was not a surprise as the structural complexity of tTET is much higher than those of sTET and dTET. Both AFM (Figure 4b) and CyroEM (Figure 4c) showed that the tTET samples contained individual tetrahedral-shaped solid particles with the expected size (in terms of the strut length, 43 nm by design, 53 nm by AFM, 42 nm by Cryo-EM), which is significantly larger than the size of dTET. Efforts to perform 3D single-particle reconstruction from the CryoEM images was not successful, which might be the result of the following two facts: (i) Compositional heterogeneity. The tTET assembly yield was low, and it was also difficult to distinguish the fully assembled complex from those complexes lacking several strands/motifs. Thus, a certain compositional heterogeneity existed among the observed DNA particles. (ii) Structural heterogeneity. As we discussed before, the connections between layers were not completely fixed. One layer had freedom to move relative to other layers. As the number of layers increased, the degree of such motion increased as well. Thus, the DNA particles were not in the same conformation. These two factors together prevented us from reconstructing the 3D structure of tTET.

DNA nanocages can be easily modified to respond to chemical cues, such as reversible assembly/disassembly¹¹ or reversible switching of the porosity.¹² The key molecular event is dissociation of a short DNA duplex. It can be triggered by several strategies, such as toehold-initiated strand displacement,¹³ competition of ligand–aptamer binding,^{14,15} or other chemical-induced strand displacement.¹⁶ In this work, to achieve ATP-responsive layer separation between TET¹ and TET², we introduced an ATP-signaling aptamer¹⁷ into the linkage between TET¹ and TET² (Figure 5a). Specifically, the ATP aptamer was introduced into the single-stranded tail on TET². The tail on TET¹ was partially complementary to the tail

on TET². In the absence of ATP, the two sets of tails hybridized with each other, leading to the formation of dTET. It should be noted that part of the aptamer sequence was within the linkage duplex. In the presence of ATP, the aptamer–ATP binding would favorably compete with the linkage duplex formation, resulting in dissociation of the linkage duplex and subsequently the separation of TET¹ and TET². Native PAGE confirmed that the ATP-responsive strategy worked (Figure 5b). Comparison of Figure 5b with Figure 2 shows that the modified, ATP-responsive dTET had almost the same electrophoretic mobility as the original dTET did. After exposure to 1 mM ATP, a biologically relevant ATP concentration,¹⁸ two distinct bands appeared. They migrated at the same speed as inside TET¹ and outside TET², respectively. This result demonstrated that ATP could indeed induce layer separation of dTET.

In summary, we have developed a strategy to assemble a Russian-doll-like, semisolid multilayered DNA nanocage, which has been further modified to respond to a chemical cue. The layer-by-layer assembly strategy used here provides a generally applicable strategy for achieving high structural complexity. We expect that it can be readily applied to other DNA nanostructures, including DNA origami and single-strand-tile structures. In addition, the responsive property demonstrated in this work suggests a way for controllable release of cargos enclosed in nanocages.

■ ASSOCIATED CONTENT

S Supporting Information

Materials and methods and additional experimental data. This material is available free of charge via the Internet at <http://pubs.acs.org>.

■ AUTHOR INFORMATION

Corresponding Author

*mao@purdue.edu

Notes

The authors declare no competing financial interest.

■ ACKNOWLEDGMENTS

We thank NSF for supporting this research. The CryoEM images were taken at the Purdue Biological Electron Microscope Facility.

■ REFERENCES

- (1) Seeman, N. C. *Nature* **2003**, *421*, 427–431.
- (2) Lin, C.; Liu, Y.; Yan, H. *Biochemistry* **2009**, *48*, 1663–1674.
- (3) Aldaye, F. A.; Palmer, A. L.; Sleiman, H. F. *Science* **2008**, *321*, 1795–1799.
- (4) Douglas, S. M.; Bachelet, L.; Church, G. M. *Science* **2012**, *335*, 831–834.
- (5) Lo, P. K.; Karam, P.; Aldaye, F. A.; McLaughlin, C. K.; Hamblin, G. D.; Cosa, G.; Sleiman, H. F. *Nat. Chem.* **2010**, *2*, 319–328.
- (6) He, Y.; Ye, T.; Su, M.; Zhang, C.; Ribbe, A. E.; Jiang, W.; Mao, C. *Nature* **2008**, *452*, 198–201.
- (7) Andersen, E. S.; Dong, M.; Nielsen, M. M.; Jahn, K.; Subramani, R.; Mamdouh, W.; Golas, M. M.; Sander, B.; Stark, H.; Oliviera, C. L. P.; Pedersen, J. S.; Birkedal, V.; Besenbacher, F.; Gothelf, K. V.; Kjems, J. *Nature* **2009**, *459*, 73–76.
- (8) Williams, S.; Lund, K.; Lin, C.; Wonka, P.; Lindsay, S.; Yan, H. *Lect. Notes Comput. Sci.* **2009**, *5347*, 90–101.
- (9) Tang, G.; Peng, L.; Baldwin, P. R.; Mann, D. S.; Jiang, W.; Rees, I.; Ludeke, S. J. *J. Struct. Biol.* **2007**, *157*, 38–46.
- (10) Goddard, T. D.; Huang, C. C.; Ferrin, T. E. *J. Struct. Biol.* **2007**, *157*, 281–287.
- (11) Liu, Z.; Li, Y.; Tian, C.; Mao, C. *Biomacromolecules* **2013**, *14*, 1711–1714.
- (12) Zhang, C.; Tian, C.; Li, X.; Qian, H.; Hao, C.; Jiang, W.; Mao, C. *J. Am. Chem. Soc.* **2012**, *134*, 11998–12001.
- (13) Zhang, D. Y.; Winfree, E. *J. Am. Chem. Soc.* **2009**, *131*, 17303–17314.
- (14) Tang, Z.; Mallikaratchy, P.; Yang, R.; Kim, Y.; Zhu, Z.; Wang, H.; Tan, W. *J. Am. Chem. Soc.* **2008**, *130*, 11268–11269.
- (15) Nutiu, R.; Li, Y. *J. Am. Chem. Soc.* **2003**, *125*, 4771–4778.
- (16) Liu, Z.; Mao, C. *Chem. Commun.* **2014**, *50*, 8239–8241.
- (17) Huizenga, D. E.; Szostak, J. W. *Biochemistry* **1995**, *34*, 656–665.
- (18) Beis, I.; Newsholme, E. A. *Biochem. J.* **1975**, *152*, 23–32.